MRI visualization of neuroinflammation using VCAM-1 targeted paramagnetic micelles

MRI visualization of neuroinflammation using VCAM-1 targeted paramagnetic micelles

Garello Francesca, [1] Pagoto Amerigo, Arena Francesca, Buffo Annalisa,[2,3] Alberti Diego, and Terreno Enzo[1]

[1] Molecular & Preclinical Imaging Centers, Department of Molecular Biotechnology and Health Sciences, University of Torino, Via Nizza 52, 10126 Torino, Italy
[2] Department of Neuroscience Rita Levi-Montalcini, University of Turin, 10126 Turin, Italy
[3] Neuroscience Institute Cavalieri Ottolenghi, Regione Gonzole 10, 10043 Orbassano, Turin, Italy

Abstract

The detection of neuroinflammatory processes with innovative and non-invasive imaging techniques, such as Magnetic Resonance Imaging (MRI), could be of great help to deeply investigate neurodegenerative diseases'onset and progression. However, as the anatomical alterations at the initial stages of degeneration are limited, the use of contrast agents targeting selected markers of inflammation, such as Vascular Cell Adhesion Molecule (VCAM-1) over-expression, is envisaged. In the herein reported work VCAM-1 targeted paramagnetic micelles were designed and tested in a mouse model of acute neuroinflammation. The nanosystem obtained, with a longitudinal relaxivity of 35 $s^{-1}mM_{Gd}^{-1}$ at 1T, was administered in mice bearing LPS-induced striatal inflammation. The T1 signal enhancement calculated over pre images showed an increase at 24h *p.i.* of 39.3 ± 4.4 % only in the inflamed striatum, with a T1 signal enhancement over the healthy contralateral hemisphere of 31.1 ± 4.5 %. The inflamed region was clearly identified and detected only after targeted micelle administration and *ex-vivo* histological studies confirmed the presence of an active targeting. Scrambled micelles and the clinically approved contrast agent MultiHance® were also tested, resulting in a T1 signal enhancement over pre images of 18.9 ± 2.2 and 13.4 ± 2.7 %, respectively, probably due to passive extravasation only. In conclusion this originally designed nanosystem allows for the detection of neuroinflammation, with a higher T1 signal enhancement and a more precise localization in comparison to the routinely used MultiHance®, paving the way to the potential study of the role of neuroinflammation in various neurological disorders.

Introduction

Neuroinflammation is an active multifaceted adaptive process. It has been detected in infectious brain diseases as well as following central nervous system (CNS) traumatic injury, and, more recently, in patients affected by various neurodegenerative diseases.1-3 The main features of this dynamic process are: (i) changes in the vasculature (increased blood flow and vascular permeability), (ii) activation of resident immune competent cells, (iii) infiltration of mobile cells of the immune system (neutrophils, macrophages, lymphocytes) and (iv) cytokine production.4,5 This orchestrated machinery would have the purpose of limiting the extent of the disease, clearing tissue damage and supporting repair and regeneration; but at the same time, it could lead to the boosting and perpetuation of inflammation.6-8 The precise mechanisms regulating and driving this frail equilibrium are still not completely clarified. Indeed the close relationship between neuroinflammation and the onset and development of many neurodegenerative diseases, such as Alzheimer's disease, Parkinson's disease, multiple sclerosis, Huntington's disease, or neurological disorders like epilepsy, is becoming more and more undeniable.9-15 Since these disorders are affecting millions of people worldwide and their prevalence is expected to raise in the next decades,5 the need for specialized non invasive imaging techniques is increasing in order to better clarify the role and the spatio-temporal correlation between inflammation and degeneration. So far, in clinics, most of the imaging techniques employed allowed for the diagnosis of neurodegenerative diseases only at later stage of progression, hence limiting the treatment outcome.16-18 Various targeted Positron Emission Tomography (PET) tracers have been designed and tested in clinics, as the ^{11}C-Pittsburgh Compound B ([^{11}C]-PIB), an analogue of thioflavine displaying a remarkable affinity for beta-amyloid plaques,19 [^{18}F]FDDNP, for the *in vivo* imaging of neurofibrillary tangles,20 and ^{11}C PK1195 targeting translocator protein (TSPO) over

expression, associated to microglial activation.21 Despite the great sensitivity of PET imaging and the possibility to obtain quantitative information, these compounds, due to their lipophilic nature, display a considerable non specific binding, resulting in remarkable signal overlap with control patients.22-25 In addition PET imaging is characterized by high costs, reduced half-life time of the tracers and limited follow up of the patients due to use of gamma radiations?. Magnetic Resonance Imaging (MRI), due to its outstanding spatial resolution, moderate cost-effectiveness, relatively slow kinetics of probes and lack of radiation exposure, could be regarded as the technique of choice for neuroimaging. The diagnosis of different neurological disorders, indeed, can be performed through the MR assessment of volume changes in specific brain regions, as hippocampal atrophy in Alzheimer's Disease (AD) or caudate head atrophy in Huntington's disease.26,27 In addition the presence of demyelinating plaques, in multiple sclerosis (MS), can be highlighted through diffusion weighted imaging (DWI), T_1 and T_2 weighted ($T1_w$ and $T2_w$) MR imaging, whilst Parkinson's disease (PD) can be diagnosed through the detection of the loss of the normal swallow tail appearance of susceptibility signal pattern in the substantia nigra.28-31 These are just some examples on how MRI can help in the identification of different neuropathologies, assess response to treatment and try to determine the disease pattern. However, routine structural neuroimaging evaluations are normally based on the observation of late features in the progression of the disease. Therefore developing new MRI approaches for early and specific recognition of neurological diseases at the prodromal stages is of crucial importance. In light of the low sensitivity that characterizes magnetic resonance imaging and of the difficulties encountered by the mostly hydrophilic paramagnetic probes in overcoming an intact blood brain barrier (BBB), a suitable strategy to obtain a considerable signal is the development of molecules targeting the changes in the vasculature. More in details, in the event of neuroinflammation, infiltration of immune cells from the bloodstream into CNS parenchyma occurs through a sequential and coordinated process involving tethering, rolling, adhesion and transmigration of leucocytes across the BBB.32,33 Each step involves interaction of BBB endothelial cells and leukocytes via endothelial expression of Cell Adhesion Molecules (CAMs), such as intercellular CAM-1 (ICAM-1) and vascular CAM-1 (VCAM-1). VCAM-1 is not constitutively expressed on the endothelium but is up-regulated upon endothelial activation, thus being an attractive molecular imaging target of early cerebral inflammation, easily accessible to blood borne contrast agents.34-36 Microparticles of iron oxide (MPIO) were already conjugated to mouse monoclonal VCAM-1 antibody (VCAM-MPIO) to generate highly specific hypointense contrast effects delineating the architecture of activated cerebral blood vessels.37 However, so far Gd-containing nanosystems targeting the over expression of VCAM-1 have not been tested yet in the visualization of CNS inflammation. Indeed the use of positive contrast agents is advisable to unequivocally locate the inflamed region, avoiding signal misunderstandings due to the presence of hemorrhages, air or abnormal mineral substances accumulation.38 In addition, as MPIO are avidly taken up from the immune system cells, the use of stealthier particles is desirable to increase the blood half-life time of the system and increase the targeting efficiency. In the herein reported work VCAM-1 targeted paramagnetic micelles, developed by our group,39 were tested in a murine model of acute neuroinflammation in order to investigate their potential application in the precocious detection of neurodegenerative processes.

Experimental

2.1 Chemicals

bEnd.3 cells [BEND3] (ATCC® CRL-2299) were obtained by ATCC (LGC Standards S.r.l., Sesto San Giovanni (MI) Italy) at passage 24 and used until passage 30. All materials necessary for cell culture were purchased from Lonza (Lonza Sales AG, Verviers, Belgium). 1,2-Distearoyl-sn-glycero-3-phospho-ethanolamine-N-[amino(poly(ethylene glycol)2000] ammonium salt (DSPE-PEG2000-NH2), 1,2-distearoyl-sn-glycero-3-phosphoethanolamine-N- [methoxy(polyethylene glycol)-2000] ammonium salt (DSPE-PEG2000-OMe), 1,2-dioleoyl-sn-glycero-3-phosphoethanolamine-N-

(lissamine rhodamine B sulfonyl) (ammonium salt) (Rho-DOPE) were obtained from Avanti Polar Lipids (Alabaster, USA). Gd-DOTAMA(C18)$_2$ was synthesized as described elsewhere.40 Rat monoclonal antibody [M/K-2] to VCAM1 (FITC) was purchased by Abcam (Cambridge, UK). Rat anti mouse F4/80 antibody, clone Cl:A3-1, and rat anti-mouse CD31, Clone MEC 13:3, were supplied by Serotec Abd (Kidlington, UK) and BD Pharmingen (Erembodegem, Belgium), respectively. Goat anti-Rat IgG (H+L) Secondary Antibody Alexa Fluor 488 was purchased by Invitrogen (Carlsbad, California, USA), respectively. Lipopolysaccharides from *Escherichia coli* 055:B5 and Hoechst 33342 were supplied by Sigma-Aldrich Co. LLC (Milano, Italy).

2.2 Animal Care and Use

C57BL/6J female mice (8-12 weeks old) were obtained from the animal facility of the Molecular Biotechnology Center (Turin). All the procedures were approved by the local institutional animal care committee (Ethical Committee of University of Turin). Anesthesia was provided by intramuscular injection of a combination of 20 mg/kg tiletamine/zolazepam (Zoletil 100; Virbac, Milan, Italy) and 5 mg/kg xylazine (Rompun; Bayer, Milan, Italy).

2.3 Micelle Preparation and Characterization

VCAM-1 targeted micelles were prepared through the lipid film hydration method, followed by sonication, using the following composition: DSPE-PEG2000, Gd-DOTAMA(C18)$_2$, DSPE-PEG2000-peptide (targeted or scrambled) and Rho-DOPE in a molar ratio of 57.5:40:2:0.5, with a final lipid concentration of 15 mg/mL. The solid phase peptide synthesis of the targeted or scrambled peptide and its conjugation to the phospholipid DSPE-PEG2000 is reported in a previously published work.39 The suspension was sonicated twice for 90 s (power 50 W, Sonicator Bandelin Sonoplus HD 2070, Berlin, Germany). During sonication, the mixture was cooled with ice to keep the temperature under 10 °C. The mean hydrodynamic ratio and polydispersity index were determined by Dynamic Light Scattering (DLS) (Malvern, Zetasizer). The millimolar longitudinal relaxivity (r_1) of the paramagnetic nanoparticles was measured at 0.5 T (Stelar Spinmaster Spectrometer, Pavia, Italy). The concentration of Gd(III) in the micelle suspension was determined by relaxometry.41

2.4 Estimation of VCAM-1 receptor expression

First, the expression of VCAM-1 receptor in the cell line before and after treatment with Tumor Necrosis Factor alpha (TNF-alpha) was investigated by fluorescence-activated cell sorting (FACS) analysis. To this purpose bEnd.3 cells were cultured in complete Dulbecco's Modified Eagle's Medium (DMEM) until confluence was reached and then were either treated for 4 hours with TNF alpha (50 ng/mL) or left in complete growth medium. Subsequently cells were detached with Versene (EDTA) 0.02%, divided in different aliquots ($0.2x10^6$ cells/tube) and resuspended in 100 µL of Phosphate Buffered Saline enriched with 0.1% Bovine Serum Albumin (PBS-BSA). Incubation with FITC conjugated anti VCAM-1 antibody was carried out for 1 h in ice. Mouse IgG1-FITC isotype was used as control. Cells were rinsed in PBS-BSA to remove unbound material and finally resuspended at a concentration of $0.6x10^6$ cells/mL in PBS-BSA. The presence of VCAM-1 receptor was investigated on a Flow Cytometer (Becton Dickinson, FACS Calibur).
To determine the mean number of VCAM-1 receptors/cell the same experiment was repeated without BSA in order to avoid interactions with serum proteins. To this end, after FACS analysis, cells were sonicated in ice (20 W) for 30 s. The protein concentration was then measured in each sample using the commercial Bradford assay (Bio-rad Protein Assay, Hercules, CA, USA) by means of a spectrophotometer (6715 UV/Vis Spectrophotometer Jenway). Since the number of cells is proportional to the protein concentration, this value was converted into the corresponding cell number

($Ncells$) using a dedicated calibration curve. Then the fluorescence of each sample was measured in a solution of Triton X-100 0.1% (v/v) in PBS using the spectro-fluorometer (Fluoromax-4-Horiba Scientific) with λ_{exc} 492 nm and λ_{em} 517 nm. The fluorescence value of cells incubated with the mouse isotype was considered as aspecific contribution and subtracted from the measured fluorescence intensity values. A calibration curve of standard FITC (fluorescence intensity vs. concentration) was used to correlate the normalized intensity values to the moles of FITC. Finally the number of VCAM-1 receptors/bEnd.3 cell was estimated as follows:

$$\frac{VCAM1_{receptors}}{bEnd.3\ Cell} = [([FITC]/7)\ x\ N_A]/Ncells$$

where 7 is the number of FITC molecules/antibody and N_A is the Avogadro constant.

2.5 In vitro assays

An *in vitro* assay was performed to evaluate the possibility and specificity of targeted micelle binding to VCAM-1 receptors in brain endothelial cells. To achieve this goal bEnd.3 cells were cultured until confluence in two different T175 flasks, then to one flask 50 ng/mL of TNF alpha were added for 4 hours to induce VCAM-1 over-expression, whilst to the other flask fresh complete growth medium was added. Cells were then detached with Versene (EDTA) from both flasks and divided into three aliquots. The first aliquot was kept as control, the second and third ones were incubated with either VCAM-1 targeted micelles or scrambled micelles at 2 mM Gd^{3+} concentration. Incubation was performed at 4°C for 30 minutes in order to allow receptor binding and minimize micelle uptake. Subsequently cells were thoroughly washed, resuspended in 50 µL of PBS, transferred into glass capillaries and centrifuged to obtain cell pellets. The capillaries were then inserted into an agar phantom in order to mimic tissues and imaged at 7.0 T with a NMR Bruker Avance 300. *T1w* Multi Slice Multi Echo MSME (Echo Time (TE)/ Repetition Time(TR)/ Number of Averages(NAV) 3.68/200/12, Matrix 128x128) and *T2w* RARE (TE/TR/NAV/Rare Factor(RF) 3.68/200/12/32, Matrix 128x128) sequences were acquired. T1 measurement of the cell phantom was performed varying the repetition time from 50 to 8000 ms (TE/TR/NR 3.68/50-8000/10, Matrix 128x128). The T1 of each sample was then calculated by means of ROI selection directly on the acquired images. The longitudinal relaxation values (*R1* = 1/T1) were also calculated. At the end of the acquisition the samples were recollected, suspended in 200 µL of PBS and sonicated at 20 W for 30 s, in ice. Then the amount of proteins was measured with the Bradford assay and the related number of cells estimated as reported in *paragraph 2.4*. To quantify the amount of gadolinium in each sample, cell extracts were digested with concentrated HNO_3 (70%, 1 mL) under microwave heating (MilestoneMicroSYNTH Microwave labstation), recollected in ultrapure milli-Q water and analyzed by inductively coupled plasma mass spectrometry (ICP-MS; element-2; Thermo-Finnigan, Rodano (MI), Italy). The mean Gd^{3+} content in each cell was then calculated as mol of Gd^{3+}/cell. Moreover the normalized relaxivity *r1p* of each sample *s* was calculated as:

$$r1p_s = \frac{R1_s - 0.40}{[Gd^{3+}]}$$

To visualize VCAM-1 targeted micelle binding of VCAM-1 receptor in bEnd.3 cells, the cells were plated in ibidi® µ-slide wells ($1x10^4$ cells/well) and cultured until confluence. Then in 4 wells cells were treated with TNF-alpha to induce VCAM-1 receptor over-expression, whereas in the other four wells complete growth medium was added. After 4 hours cells were washed twice with PBS and incubated with VCAM-1 targeted micelles (0.12 mM Gd^{3+}) for 30 min at 4°C. At the end of incubation cells were thoroughly washed with PBS, fixed with 4% Formalin (15 min, RT) and stained with Hoechst to visualize nuclei. Confocal microscopy images were acquired with a Leica SP5

confocal microscope ($laser_1$ excitation 405 nm, acquisition window 415–480 nm, $laser_2$ excitation 561 nm, acquisition window 580–675 nm, to visualize Hoechst and rhodamine, respectively).

2.6 Half-life time of VCAM-1 targeted micelles

The blood half-life time of VCAM-1 targeted micelles was investigated in healthy C57BL/6J female mice (n=3). Micelles were administered trough tail vein injection at 0.05 $mmol_{Gd3+}$/Kg body weight. At different time points post injection (5, 15, 30 min, 1, 2, 4 and 24 h) a micro aliquot of blood was collected from the tail vein. 20 µL of Heparin (500 UI/mL) were added to each sample to avoid coagulation. The volume of blood collected at each time was quantified, then the samples were digested with concentrated HNO_3 (70%, 1 mL) under microwave heating, recollected in ultrapure milli-Q water and analyzed by ICP-MS to measure Gd^{3+} content at each time point. Data obtained, displayed as mM Gd^{3+} concentration vs. time post injection, were fitted with a mono-exponential decay curve and the half-life time was calculated.

2.7 LPS-induced neuroinflammation model

Acute neuroinflammatory response was induced in the right striatum in 8 to 12 week-old C57BL/6J female mice (weight 18±3 g). The animals were divided into 3 different groups: neuroinflamed mice administered with VCAM-1 targeted micelles (n=8), neuroinflamed mice administered with scrambled micelles (n=4) and neuroinflamed mice administered with the clinically approved contrast agent MultiHance® (n=4). One healthy mouse and one PBS intra-striatally injected mouse were used as supplementary controls. To obtain the model, mice were anesthetized, positioned in a stereotaxic apparatus (Stoelting) and the skull was exposed. The brain of the animal was then exposed via a hole, which was drilled through the skull. A glass capillary was inserted into the right striatum using the following stereotaxic coordinates from bregma: + 0.1 mm antero-posterior, − 2.1 mm mediolateral, − 2.6 mm dorsoventral. 1 µL of lipopolysaccharide (LPS) (E. coli 026:B6, Sigma-Aldrich) in sterile phosphate buffered saline PBS at a concentration of 5 µg/µl was then infused with a pneumatic pressure injection apparatus (Picospritzer II, General Valve Corporation) over 5 min followed by a 2 minute rest period to allow the solution to diffuse into the brain prior to the removal of the capillary. For the saline control mouse the same surgery, as described above, was performed, but the vehicle only (1 µL of PBS) was injected intra-striatally. The presence of inflammation was investigated *ex-vivo* by hematoxylin and eosin staining; VCAM-1 over-expression in the inflamed striatum was assessed by confocal microscopy following staining with FITC anti VCAM-1 antibody and Hoechst (see ESI).

2.8 In vivo Magnetic Resonance Imaging

All the MR images were acquired on a Bruker Icon (1 T) equipped with a brain surface coil. Animals were recruited 24 hours post LPS injection. MRI acquisition was performed under 1 % isoflurane anesthesia. Animals were scanned before and 20 min, 4h, 24h, 48 h post injection of VCAM-1 targeted paramagnetic micelles or micelles decorated with a scramble peptide. T_2-Weighted MRI images were obtained using a RARE sequence protocol (TR/TE/NAV=2500/26.7/12). T1-weighted MRI images were acquired using a FLASH sequence (TR/TE/NAV = 75/5.8/18, field of view (FOV) = 1.2 cm). To compare the contrast obtained with VCAM-1 targeted micelles with the one obtained after the administration of the clinically approved contrast agent MultiHance®, MultiHance was injected in the tail vein, 24 hours after the induction of inflammation, at the concentration of 0.2 mmol Gd^{3+}/Kg and the animals were imaged repeatedly for 30 minutes.

2.9 Image processing and analysis

Image analysis was performed using Bruker ParaVision 5.1 imaging software. Regions of interest (ROIs) were drawn over right (inflamed) and left (non-inflamed) striatum in the imaging plan and average signal intensity was measured. The % T1 signal enhancement (% SE) over pre-images was calculated as follows:

$$\% SE = \frac{SNR_t - SNR_0}{SNR_0} x\ 100$$

where

$$SNR = \frac{Signal\ Intensity}{SD\ noise}$$

And *0* and *t* stands for before and after the injection of the contrast agent, respectively. *p* values were calculated using t-Student's test, assuming statistical significance at $p < 0.05$. All the data are reported as mean ± standard error of mean.

2.10 Biodistribution of VCAM-1 targeted micelles

Micelle homing to the main excretory organs, liver, kidneys and spleen, was followed by MRI at different time points after the administration of VCAM-1 targeted micelles (n=3). 24 hours post injection the animals were sacrificed and the liver, spleen, kidneys, lungs, left and right cerebral hemispheres were excised, weighted and digested in concentrated nitric acid (70%) under microwave heating, recollected in ultrapure milli-Q water and analyzed by ICP-MS to measure Gd^{3+} content. The mg of Gd^{3+}/g_{organ} were calculated. Moreover an estimation of the percentage of residual Gd^{3+} in each organ according to the administered dose was evaluated in all the excised organs as follows:

$$\% Gd = \frac{mol\ Gd_{g\ organ}\ x\ g\ organ}{mol\ Gd\ administered} x\ 100$$

2.11 Ex-vivo studies

To investigate the presence of VCAM-1 targeted micelles in the inflamed brain regions, 24 hours post administration of the nanosystem the animals (n=2) were sacrificed following MRI acquisition and the brain was extracted and cryopreserved at -80°C until cryostat sectioning. Slices (20 µm thickness) were cut using a Leica CM 1950 cryostat and fixed in absolute ethanol for 5 min. Then slices were rinsed with PBS and nuclei were stained with Hoechst ($8x10^{-5}$ mg/mL, 10 min incubation). After a fast washing in bidistilled water, slices were mounted using ProLong® Gold Antifade Mountant (TermoFisher Scientific, Waltham, Massachusetts, USA). To visualize blood vessels CD-31 was stained, whereas to visualize microglia/peripheral macrophages anti F4/80 antibody was used. To this purpose following fixation in ethanol, slices were washed in PBS and then blocking with 10% goat serum was performed for 1h at room temperature. Subsequently the primary antibody was added to the slices in 10% goat serum and left overnight at 4°C (anti CD31 1:200 dilution, anti F4/80 1:50 dilution). The day after the slices were rinsed in PBS and staining with the secondary antibody (1:500) was carried out for 1 hour at room temperature. Three washings were performed to remove unbound material, and then nuclei were stained with Hoechst ($8x10^{-5}$ mg/mL, 10 min incubation). After a fast washing in bidistilled water, slices were mounted using ProLong®. All the slices were imaged by confocal microscopy, magnification 40x, laser excitation 405, 488, 561 nm to detect Hoechst, Alexa Fluor 488 or Rhodamine, respectively.

Results

3.1 Micelle Preparation and Characterization

VCAM-1 targeted paramagnetic micelles were prepared with the lipid thin film hydration method. Briefly, the lipids were blended in chloroform and methanol (4:1 v/v) and the solvent evaporated by means of a rotavapor. The film was then hydrated with HEPES buffer to a final lipid concentration of 15 mg/mL and sonicated to obtain a uniform and stable population. The mean size, checked by DLS, was 20 nm with a Polydispersity Index (PDI) of 0.2 ± 0.1. The longitudinal relaxivity (*r1p*) measured at 1 T, 37°C was 35 $s^{-1}mM_{Gd}^{-1}$. Micelles bearing the scrambled version of the targeting peptide did not differ significantly in size and relaxivity in comparison to the VCAM-1 addressed nanosystem. Not shown?

3.2 Estimation of VCAM-1 receptor expression

In order to investigate the potential vascular targeting of developed micelles at the blood brain barrier, the murine brain endothelial cell line bEnd.3 was chosen as *in vitro* model**.** Although these cells are reported to constitutively express VCAM-1 receptor below passage 30, stimulation with TNF-alpha further increases its expression. Flow Citometry was employed to investigate the presence of the surface receptor before and 4h after incubation with TNF-alpha. The analysis of cell samples acquired by FACS after incubation with the FITC anti VCAM-1 antibody showed a remarkable enhancement in VCAM-1 expression after treatment with TNF-alpha. (Fig.1)

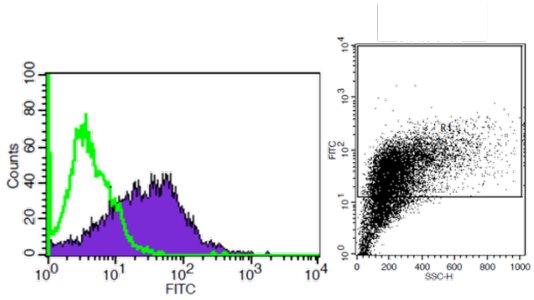

Figure 1. FACS analysis of bEnd.3 cells before (empty peak) and after (filled peak) treatment with 50 ng/mL TNF-alpha. FITC anti VCAM1 antibody was used to label the receptor.

The mean number of VCAM-1 receptors/cell was determined by fluorimetry. More in details, before and after treatment with TNF-alpha the cells were incubated with the FITC anti VCAM-1 antibody to label the receptor. Subsequently the cells were washed and sonicated, in order to measure the mg of proteins, correlated to the number of cells, and the fluorescence intensity, correlated to the amount of receptors, of each sample. Results obtained displayed near fourfold increase in VCAM-1 expression after treatment with TNF-alpha (Fig.2), thus validating the use of brain endothelial cells to study *in vitro* the potential interaction between the receptor and our newly developed nanosystem.

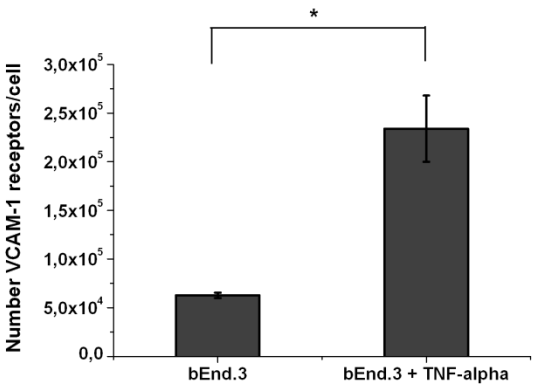

Figure 2. Mean number of VCAM-1 receptors/bEnd.3 cell before and after stimulation with TNF-alpha. The number of cells was estimated with the Bradford assay, while FITC concentration was determined by fluorimetry (* $p < 0.05$). Error bars represent SE of the mean.

3.3 In vitro assays

Targeted and non-targeted micelle affinity towards VCAM-1 was investigated *in vitro* in bEnd.3 cells. The whole experiment was carried out at 4°C in order to avoid the internalization of the nanosystem. Confocal microscopy images taken 30 min after incubation with VCAM-1 targeted micelles proved that the selected timeframe was sufficient to achieve a considerable cell membrane labeling (Fig.3). A noteworthy discrepancy in the rhodamine associated signal between naïve and activated bEnd.3 cells could be appreciated, suggesting the presence of an active membrane labeling process.

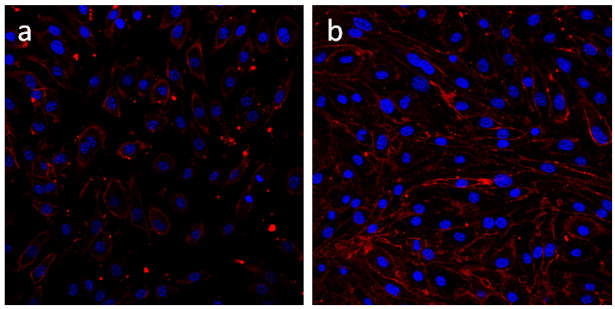

Figure 3. Confocal microscopy images of bEnd.3 cells, before (a) and after (b) activation with TNF-alpha, incubated with VCAM-1 targeted micelles. Nuclei and rhodamine signal are displayed in blue and red, respectively.

Nuclei in genere meno visibili a sn benché ci si aspetti livelli paragonabili
Forse anche un po' più piccoli? Tirare sui l segnale? Scale bar missing

To quantify the amount of receptor-bound nanosystem and the MRI signal obtained after incubation of cell samples with targeted or scrambled micelles an additional experiment was performed. More in details, cells were detached with EDTA before and after treatment with TNF-alpha and incubation with targeted or scrambled micelles (2 mM Gd^{3+}) was performed in suspension for 30 min at 4°C. At the end of the incubation cells were profusely washed to remove unbound micelles and then centrifuged into glass capillaries to obtain a cell phantom. The phantom was imaged by MR at 7.0 Tesla and the T1 of each sample was measured (Figure 4). Immediately after imaging cell pellets were recollected and sonicated to estimate the number of bEnd.3 cells using the Bradford assay and measure the exact quantity of gadolinium by ICP-MS. Hence the normalized longitudinal relaxivity (*r1p*) could be calculated for each sample. Results obtained showed very high relaxivity values, probably related to the extracellular location of the probe and to the very low concentration of gadolinium in cell pellets. Non-activated cells showed a comparable relaxivity value, around 30 $mM^{-1}*s^{-1}$, when incubated with either scrambled or targeted micelles. A faint difference, instead, was observed between activated cells incubated with VCAM-1 targeted micelles (*r1p* = 45 $mM^{-1}*s^{-1}$) or

with scrambled micelles (*r1p* = 38 $mM^{-1}*s^{-1}$). The quantification of moles of Gd(III)/bEnd.3 cell turned out to be slightly in contrast with MRI results. In particular, activated cells incubated with targeted micelles showed ca. 1.5 fold value of Gd(III) uptaken moles in comparison to cells activated with TNF-alpha but incubated with scrambled micelles ($3.3x10^{-16}$ vs. $2.2x10^{-16}$). The same relationship could be found in non-activated cells, although the number of Gd(III) moles was lower ($2.6x10^{-16}$ vs. $1.7x10^{-16}$).

Qui non occorrono/sono indicate valutazioni statistiche delle eventuali differenze, giusto?

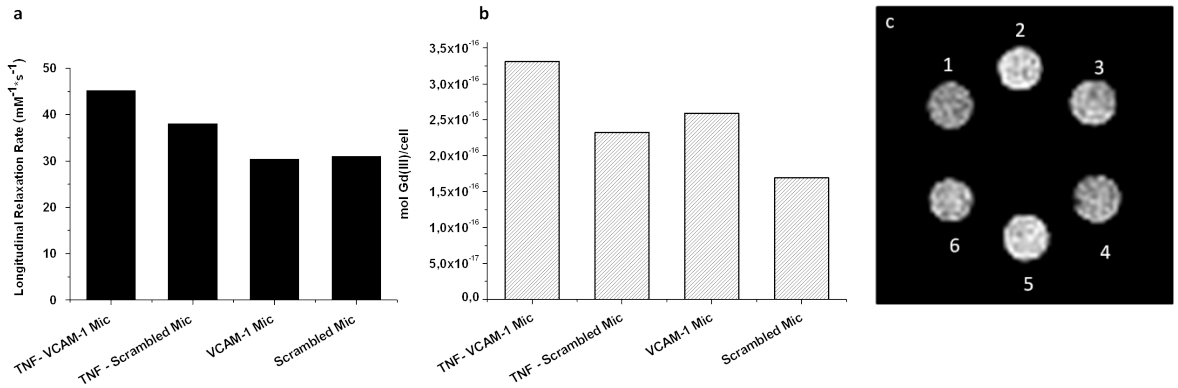

Figure 4. ***In vitro*** **study on targeted or scrambled micelle binding affinity towards VCAM-1 in activated or non-activated brain endothelial cells. a)** ***r1p*** **values of bEnd.3 cells measured at 7.0 T and normalized to ICP-MS values of Gd(III) concentration. b) moles of Gd(III) per cell calculated using Bradford assay, to determine the amount of cells, and ICP-MS, to measure Gd(III) concentration. c) T1w image of 1) activated bEnd.3 cells, 2) activated bEnd.3 cells incubated with VCAM-1 targeted micelles, 3) activated bEnd.3 cells incubated with scrambled micelles, 4) non-activated bEnd.3 cells, 5) non-activated bEnd.3 cells incubated with VCAM-1 targeted micelles and 6) non- activated bEnd.3 cells incubated with scrambled micelles. The incubation was carried out at 4°C (30 min).**

3.4 Half-life time of VCAM-1 targeted micelles

The blood half-life time of VCAM-1 targeted micelles was assessed in healthy mice (n=3). The targeting nanosystem was administered by tail vein injection, afterwards blood samples were taken at different time points, ranging from 5 min to 24 hours, mixed with heparin to avoid coagulation and quantified in terms of volume. Following digestion in concentrated nitric acid, the exact amount of Gd(III) at each time point was determined by ICP-MS. Data obtained were plotted and fitted with a mono-exponential decay curve, resulting in a mean half-life time of 376 ± 22 min, R^2= 0.99 (Figure 5).

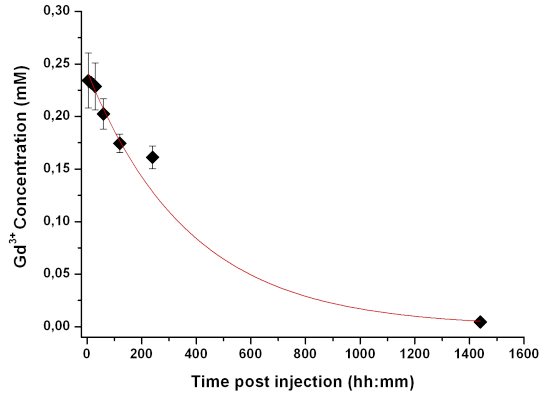

Figure 5. Mean half-life time of VCAM-1 targeted micelles assessed in healthy C57BL/6J female mice (n=3) by ICP-MS analysis of blood samples collected at different time points post injection. Error bars represent SE of the mean.

3.5 In vivo Magnetic Resonance Imaging

As *in vitro* results were promising, the potential vascular targeting of VCAM-1 targeted micelles at the blood brain barrier was investigated in a murine model of neuroinflammation. Acute neuroinflammatory response was induced in the right striatum. The presence of inflammation and the over-expression of VCAM-1 in the involved hemisphere were detectable already 24 hours after surgery by *ex-vivo* histological studies (see ESI). In the contra-lateral hemisphere almost no hallmarks of inflammation were present. The animals were recruited 24 hours after surgery, received intravenous injection of VCAM-1 targeted micelles (0.05 mmol Gd(III)/Kg body weight) and were imaged at 1.0 T at 20 min, 4h, 24h and 48 hours post injection (Figure 6) to follow micelle homing to the site of inflammation.

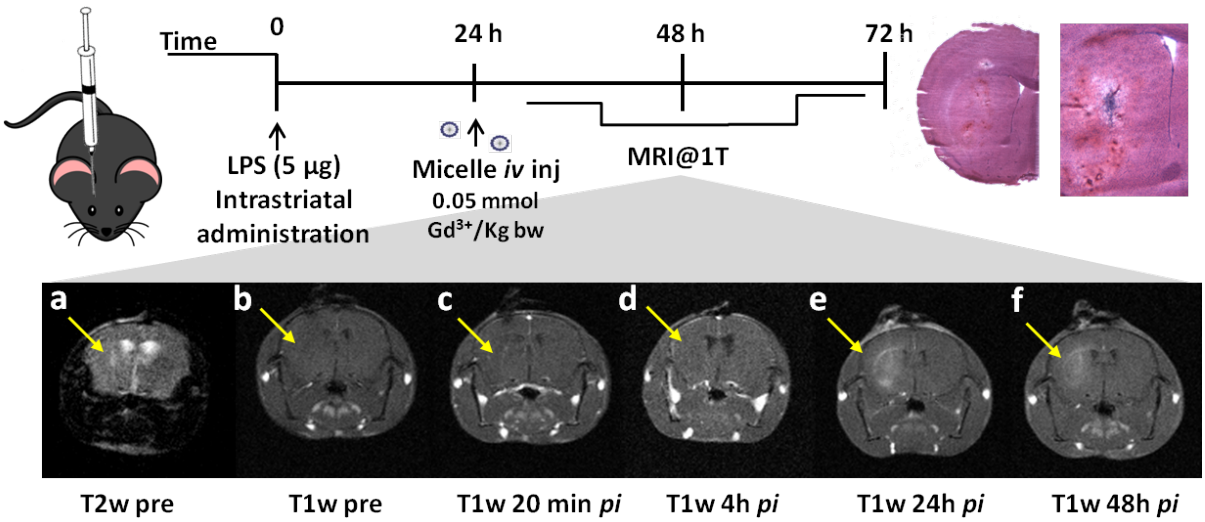

Figure 6. Top) Schematic representation of the experimental procedure: C57BL6/J mice were subjected to surgery to inject 5 µg of LPS intra-striatally in the right hemisphere; 24 h after surgery VCAM-1 targeted micelles were administered intravenously and the mice were imaged at 1T: a) T2w image pre injection, b) T1w image pre injection, c)T1w image 20 min post injection, d) T1w image 4h post injection, e) T1w image 24h post injection, f) T1w image 48h post injection. Yellow arrows indicate the inflamed region.

In T2w anatomical images a confined bright area in the operated hemisphere was occasionally detectable, suggesting the presence of an edematous region. However, only after the injection of VCAM-1 targeted micelles the real extension of the inflamed area was clearly detectable and delineable (Figure 6). In particular the T1 signal enhancement calculated over pre-images, reached its peak 24 hours post micelle injection, with a statistically significant difference between the diseased and healthy hemisphere (39.3 ± 4.4 vs. 4.1 ± 2.7 %, respectively, $p < 0.001$ - Figure 7).

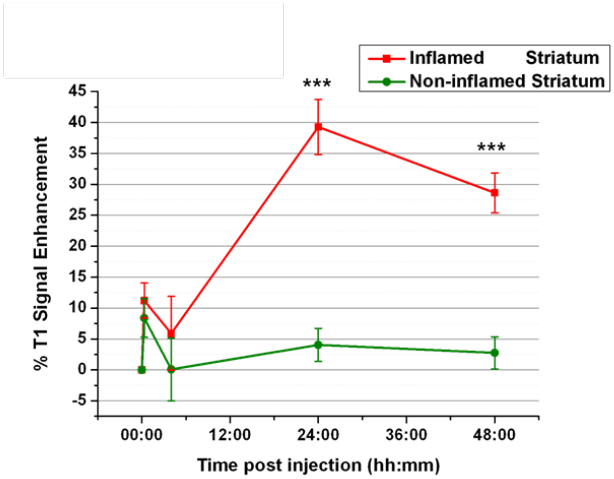

Figure 7. % T1 SE calculated over pre-images in the striatum at different time points after the injection of VCAM-1 targeted micelles. The nanosystem was administered 24 hours after the induction of inflammation (* p<0.001, n=8). Error bars represent SE of the mean.**

To ascertain the specificity of the administered nanosystem, a comparison with micelles bearing the scrambled peptide was conducted (Figure 8). Results obtained displayed a statistically significant difference between the % T1 SE obtained in the inflamed striatum after the targeted or non-targeted system administration (39.3 ± 4.4 vs 18.9 ± 2.2 %, $p < 0.01$). The signal obtained following the injection of the scrambled micelles is definitely comparable to the T1 SE detected after the administration of the routinely used MultiHance® (13.4 ± 2.7 %,), generally employed to evaluate the presence of any alterations in blood brain barrier permeability. It seems then that the contrast obtained after administration of scrambled micelles is simply related to passive extravasation, whereas for VCAM-1 targeted micelles both passive extravasation and VCAM-1 specific targeting coexist.

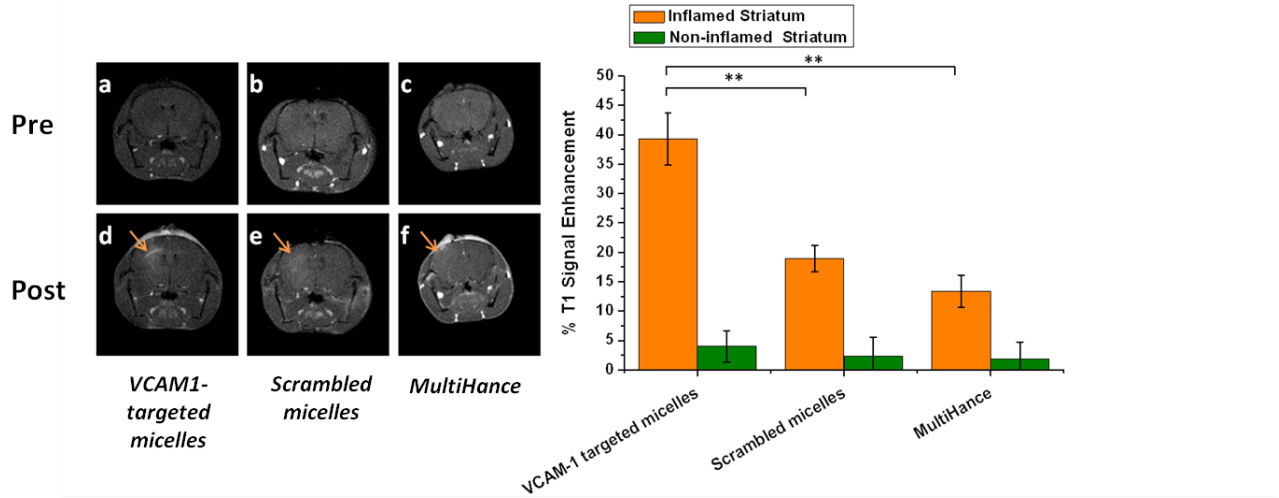

Figure 8. Left:1T MRI of neuroinflamed mice before and 24h after *iv* injection of (a,d) VCAM-1 targeted or (b,e) scrambled micelles (0.055 mmol$_{Gd3+}$/Kg), or 20 min post (c, f) MultiHance® (0.2 mmol$_{Gd3+}$/Kg) administration. Right: corresponding % T1 Signal Enhancement calculated in the diseased (orange bars) and healthy (green bars) striatum. Error bars represent SE of the mean. (p<0.01)**

2.11 Biodistribution of VCAM-1 targeted micelles

The biodistribution of the system was investigated in the main excretory organs, both *in vivo*, by MRI at 20 min, 4h and 24 hours post injection, and *ex-vivo* by ICP-MS, through quantification of Gd(III) at 24 hours post micelle injection (see ESI). Moreover, in order to estimate the amount of Gd(III) that reaches the target site, in the eventuality prospect? of judging the real power of targeted nanomedicine, the percentage of the metal found the main excretory and targeted organs 24 hours post injection was calculated over the total administered Gd(III). As displayed in figure 9 the large

majority of administered Gd(III) (44 ± 5%) resides in the liver (Figure 10). Only a small fraction was found in the inflamed region (0.30 ± 0.04% targeted micelles vs. 0.06 ± 0.01% scrambled micelles, Figure 10).

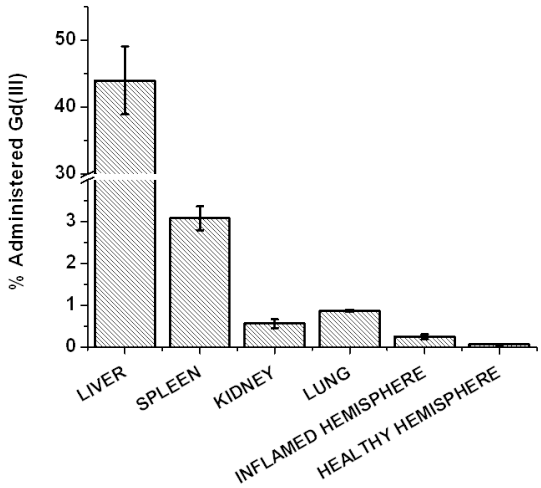

Figure 9. Quantification of % Gd^{3+} content in main excretory and target organs, 24 hours post administration of VCAM-1 targeting (green bars) or scrambled (orange bars) micelles (n=7), calculated over the total administered Gd^{3+} dosage. Error bars represent SE of the mean.

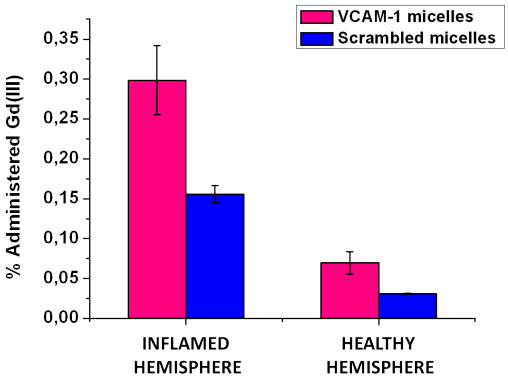

Figure 10. % $Gd3^{+}$ content quantification in right (inflamed) and left (healthy) hemisphere 24 hours after the administration of targeting (pink bars) or scrambled (blue bars) micelles (n=7) calculated over the total administered Gd^{3+} dosage. Error bars represent SE of the mean. The quantification was performed in the entire hemisphere, therefore was not limited to the main inflamed region (striatal region).

2.12 Ex-vivo studies

The targeting behaviour of VCAM-1 micelles was investigated by fluorescence microscopy. Brain slices were obtained from injected/treated mice sacrificed 24 hours post targeting micelle injection. A widespread signal originating from rhodamine was detectable in the inflamed striatum, whereas only a fable and negligible fluorescence was visible in the contra-lateral one (see ESI). Staining of vessels was performed with either anti-CD31 antibody, widely used as marker of brain endothelial cells42 (Figure 11a) or anti VCAM-1 antibody (Figure 11b-11c). Results obtained showed a massive accumulation of micelles not only stuck to the vessels, but also in the cytoplasm of adjacent and extravasating cells. Remarkably a high degree of binding to the target is still present at 24 hours post injection, corroborating the peptide targeting efficiency and supporting the idea of employing ultra small and long circulating nanosystem. As a result of confocal microscopy the idea that VCAM-1 micelle homing to the site of inflammation could be supported by immune system cells was conceived. More in details, a variable amount of micelles could be phagocytosed by bone marrow-derived (BMD) cells or activated microglia either during systemic circulation or after the eventual blood brain barrier extravasation. To better clarify this point, brain slices were stained with anti F4-

80 antibody (Figure 11d-11e) proving a massive presence of macrophages in the site of the lesion some of which loaded with the fluorescent micelles. However sporadic presence of micelles in non-macrophagic cells was still visible.

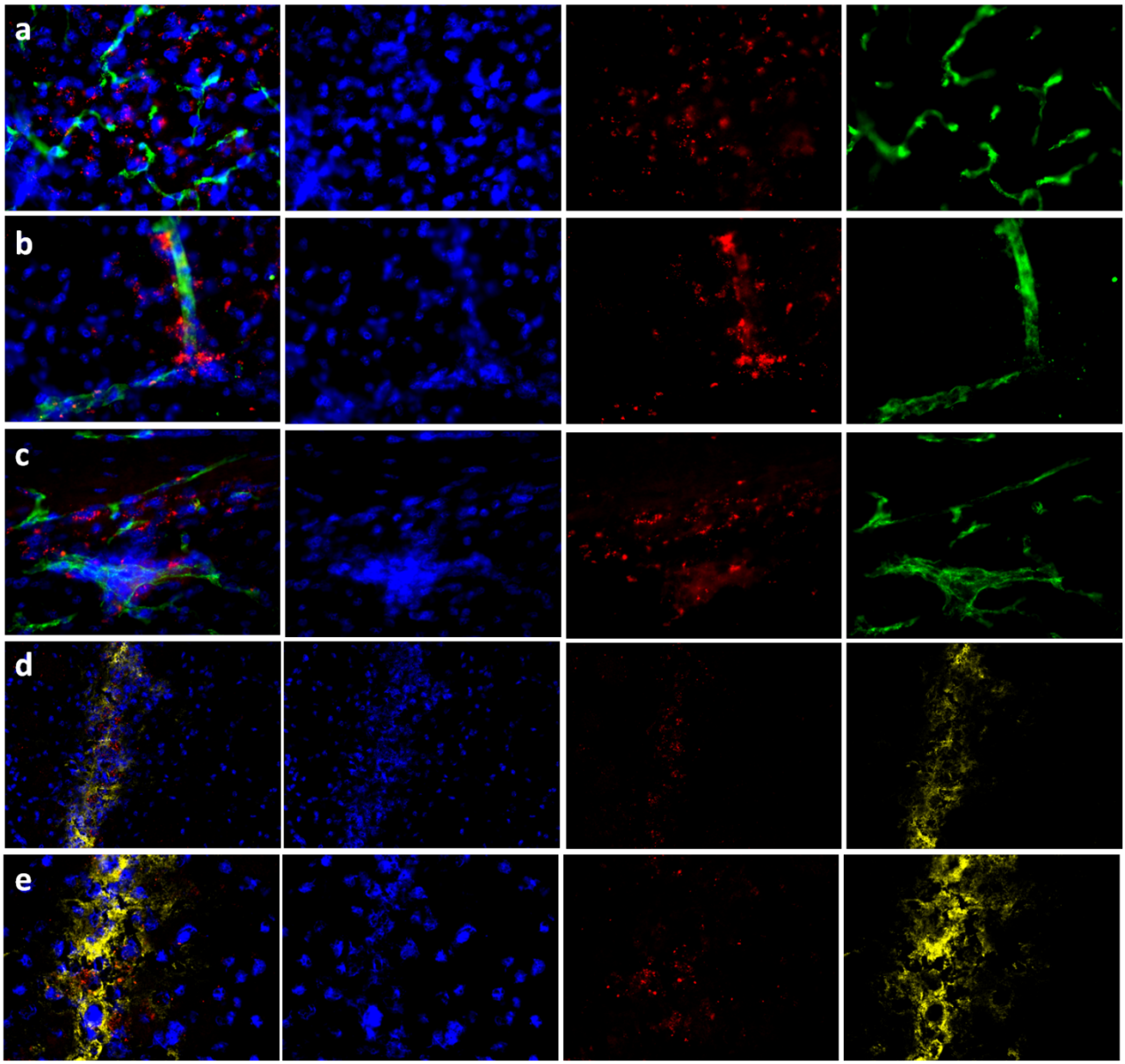

Figure 11. Confocal microscopy images of the inflamed striatum of C57BL/6J mice taken 24 hours post micelle injection. In the first column merge of the three channels is displayed, in the other columns channels are displayed separately. Nuclei are stained in blue, micelles are shown in red. a) CD31 staining (green) of brain endothelial cells; b-c) VCAM-1 staining (green) showing colocalization of micelles and related target; d-e) macrophage staining with anti F4/80 antibody (yellow) at two different magnifications.

È possibile avere un ingrandimento maggiore o produrre un imagine più chiara per sostenere colocalization di VCAM1 e micelle? Purtroppo il segnale verde e rosso non sembra sulle stesse cellule

Discussion

The development of a nanosystem targeting neuroinflammation could be of great help in the comprehension, interception and prevention of various neurological disorders. This process, in fact, is diffuse and actively involved in demyelinating and neurodegenerative diseases, stroke and malignant CNS tumors.43 As extensively reviewed by Pulli et al. 44 VCAM-1 has been selected as target to detect neuroinflammation, mainly by MRI, in manifold works. However most of the probes

developed are intended to achieve a negative MRI contrast. For instance 1 μm sized particles of iron oxide conjugated to anti-VCAM1-antibody, further referred to as VCAM1-MPIO, were successfully tested in a model of acute neuroinflammation, of autoimmune encephalomyelitis (EAE) or for earlier detection of brain metastases. 45-47 However T2 contrast agents, despite their great sensitivity, are not ideal to detect subtle neurodegenerative disorders as T2 hyper-intensities in the brain could be also associated to the presence of hemorrhagic foci, intracranial metastases, mucous- or protein-containing lesions, iron, copper or calcium deposition, turbulent flow of the Cerebrospinal Fluid (CSF), air-containing spaces, demyelination or axonal loss.48 The signal obtained with T1 contrast agents, instead is more specific and limited to the diseased area, without the occurrence of "blooming artifacts". Actually Gd-complexes are widely used in clinics to highlight BBB breakdown, but to clearly visualize a signal a micromolar accumulation of the probe is required, thus restricting the detection of inflammation to severe clinical cases and reducing the chances of visualization of mild and early-stage phenomena. So far the use of targeted T1 probes has been quite limited in literature, possibly due to the lower sensitivity associated to Gd(III) compounds in comparison to iron oxide particles. Chen et al developed a myeloperoxidase (MPO) -activatable paramagnetic sensor to detect more and confirm smaller and earlier active demyelinating lesions in the EAE model, due to the achievement of longitudinal relaxivity values around 25 $mM_{Gd}^{-1}s^{-1}$ (at 1.5 T) in the presence of high amounts of the soluble MPO enzyme.49 In this light our probe has the advantage of carrying a high payload of Gd(III) per micelle, resulting in a considerable longitudinal relaxivity value of 35 $mM_{Gd}^{-1}s^{-1}$ (at 1 T), thus raising the possibility of detecting fable and still limited inflammatory processes. The T1 signal enhancement over pre-images obtained 24 hours post micelle injection attested at around 40 %, a significant value if considered that it was calculated over the entire striatal region and not limited to a smaller and more precise region. Moreover the real extension of inflammation visible after the administration of the nanosystem was considerably higher than that perceived with mere T2 pre-contrast acquisitions or T1 images post MultiHance® administration, routinely used in clinics, thus confirming the great potentiality of the developed system.

According to our previously published work,39 a deeper pharmacokinetic investigation of the system was performed and resulted in a mean blood-half-life of targeted micelles of around 6 hours, a value in line with other pegylated nanosystems50 and remarkably different to the very short (<5 min) circulation time reported for VCAM-MPIO.47 The extended circulation time represents a great advantage to favor the binding of the peptide to the endothelial marker of inflammation and the possible extravasation of the system, while the aspecific uptake by macrophages is reduced. As further proof of this fact, the *ex-vivo* histological studies carried out demonstrated the occurrence of a strong binding between micelles and blood brain barrier capillaries, still 24 hours post injection, giving the opportunity to follow VCAM-1 expression for prolonged time windows. Even if the presence of micelles inside microglia/macrophage was detected by confocal microscopy it should be clarified if the uptake occurred during circulation or directly in the site of inflammation. However this finding is not disturbing as macrophage infiltration and activation is another important aspect associated to neuroinflammation, hence the signal in diseased sites could be even increased. Obviously a strong point for the clinical translation of these micelles would be the accurate study of times and ways of Gd(III)-complexes clearance from the brain, to allow repeated scans and avoid toxicity effects. Moreover another important consideration regards the real potentiality of targeted nanosystems, as it is, at present, a great matter of debate.51 We found that just the 0.3% of injected Gd(III) reached the targeting site, against a remarkable liver aspecific accumulation (45 % of injected gadolinium). The strategy to possibly increase the accumulation of the probe at the targeting site and simultaneously reduce the uptake by RES organs could be a sort of pre-saturation of Kupffer cells through the administration of a lipid non-contrastophor mixture before the injection of the smart nanosystem. This approach would be of great interest in view of the exploitation of VCAM-1 targeted micelles for theranostics purposes, as a high number of works already reported the loading of various drugs in micelles.52-54 Loading VCAM1-micelles with anti-inflammatory or anti-cancer molecules would allow the monitoring and treatment of neuro-inflammatory disorders or CNS malignant cancer,

respectively. The development of alternative paramagnetic VCAM-1 targeting nanosystems, such as liposomes, could also be pursued in order to select the best performing nanostructure depending on the pathology. Moreover, given the high potentiality of the system, it will be tested in finer animal models of neurodegeneration, to better investigate the relationship between inflammation and degeneration in the central or peripheral nervous tissue.

In summary, in this work paramagnetic VCAM-1 targeted micelles were developed and tested for their efficiency in targeting VCAM-1 expression. The *in vitro* data showed the target potentiality of micelles to VCAM-1 receptors in bEnd.3 cells, by both MRI and confocal microscopy. The *in vivo* data demonstrated, in a mouse model of neuroinflammation, that the accumulation of targeting nanosystem in the diseased site is significantly higher in comparison to that obtained with the scrambled nanosystem or to the signal detectable following the administration of the clinically approved contrast agent MultiHance®. In particular, it is possible to observe at 24 h *p.i.*, thanks to the quite long blood half-life of the stealth nanosystem, a visible T1 contrast enhancement that reaches 40% in the damaged hemisphere. Our data also suggests, besides a vascular target and limited passive extravasation of the micelles, an immune-mediated brain accumulation across the BBB. Results here obtained could then pave the way to interesting future diagnostic/therapeutic applications envisaging the loading of neuroprotective or even anti-cancer drugs inside the hydrophobic core of the micelles.

Acknowledgements
European Union's FP7/2007–2013 under grant agreement no. HEALTH-F2-2011-278850 (INMiND) is gratefully acknowledged.

Electronic Supporting Information (ESI)
The Supporting Information is available…..

List of abbreviations

AD Alzheimer's Disease
BBB Blood Brain Barrier
BMD Bone Marrow-Derived
BSA Bovine Serum Almbumine
CNS central nervous system
CSF Cerebrospinal Fluid
DLS Dynamic Light Scattering
DWI diffusion weighted imaging
EAE Autoimmune Encephalomyelitis
FACS fluorescence-activated cell sorting
FOV Field of View
ICP-MS Inductively Coupled Plasma Mass Spectrometry
LPS Lipopolysaccharides
MPIO Microparticles of Iron Oxide
MPO Myeloperoxidase
MRI Magnetic Resonance Imaging
MS Multiple Sclerosis
NAV Number of Averages
NMR Nuclear Magnetic Resonance
PBS Phosphate-buffered saline

PDI Polydispersity Index
PET Positron Emission Tomography
RF Rare Factor
ROI Regions Of Interest
SE Signal Enhancement
$T1_w$ T_1 weighted
$T2_w$ T_2 weighted
TE Echo Time
TNF-alpha Tumor Necrosis Factor alpha
TR Repetition Time
TSPO translocator protein
VCAM-1 Vascular Cell Adhesion Molecule

References

1. Amor S, Puentes F, Baker D, van der Valk P. Inflammation in neurodegenerative diseases. *Immunology*. 2010;129(2):154-169.
2. Faden AI, Loane DJ. Chronic neurodegeneration after traumatic brain injury: Alzheimer disease, chronic traumatic encephalopathy, or persistent neuroinflammation? *Neurotherapeutics* (2015) 12:143-150.
3. Ellwardt E, Zipp F. Molecular mechanisms linking neuroinflammation and neurodegeneration in MS. […]
4. Ory D, Cele+n S, Verbruggen A, Bormans G. *PET radioligands for in vivo visualization of neuroinflammation*. *Curr Pharm Des*. 2014; 20(37):5897-913.
5. Jacobs AH, Tavitian B. Noninvasive molecular imaging of neuroinflammation. J Cereb Blood Flow Metab 2012; 32: 1393-415.
6. Morales I, Guzmán-Martínez L, Cerda-Troncoso C, Farías GA, Maccioni RB. Neuroinflammation in the pathogenesis of Alzheimer's disease. A rational framework for the search of novel therapeutic approaches. *Frontiers in Cellular Neuroscience*. 2014;8:112.
7. Wilcock DM. A Changing Perspective on the Role of Neuroinflammation in Alzheimer's Disease. *International Journal of Alzheimer's Disease*, vol. 2012, Article ID 495243, 7 pages, 2012. doi:10.1155/2012/495243
8. Quarantelli M. MRI/MRS in neuroinflammation: methodology and applications. Clinical and Translational Imaging. 2015;3:475-489. doi:10.1007/s40336-015-0142-y.
9. Witte ME, Geurts JJ, de Vries HE, van der Valk P, van Horssen J. Mitochondrial dysfunction: a potential link between neuroinflammation and neurodegeneration? Mitochondrion. 2010;10(5):411-8.
10. Heneka MT et al. Neuroinflammation in Alzheimer's disease. Lancet Neurol. 2015 Apr;14(4):388-405.
11. Frank-Cannon TC, Alto LT, McAlpine FE, Tansey MG. Does neuroinflammation fan the flame in neurodegenerative diseases? Mol Neurodegener. 2009 Nov 16;4:47.
12. Hirsch EC, Hunot S. Neuroinflammation in Parkinson's disease: a target for neuroprotection? Lancet Neurol. 2009; 8(4):382-97.
13. Haider L, Zrzavy T, Hametner S, et al. The topograpy of demyelination and neurodegeneration in the multiple sclerosis brain. *Brain*. 2016;139(3):807-815.

14. Crotti A, Glass CK. The choreography of neuroinflammation in Huntington's disease. Trends Immunol. 2015 Jun;36(6):364-73.
15. Aronica E, Crino PB. Inflammation in epilepsy: clinical observations. Epilepsia. 2011 May;52 Suppl 3:26-32.
16. Agrawal M, Biswas A. Molecular diagnostics of neurodegenerative disorders. *Frontiers in Molecular Biosciences*. 2015;2:54. doi:10.3389/fmolb.2015.00054.
17. Mueller SG, Weiner MW, Thal LJ, et al. Ways toward an early diagnosis in Alzheimer's disease: The Alzheimer's Disease Neuroimaging Initiative (ADNI). *Alzheimer's & dementia: the journal of the Alzheimer's Association*. 2005;1(1):55-66. doi:10.1016/j.jalz.2005.06.003.
18. Stoessl AJ. Neuroimaging in the early diagnosis of neurodegenerative disease. *Translational Neurodegeneration*. 2012;1:5.
19. Landau SM, Breault C, Joshi AD, et al. Amyloid-β Imaging with Pittsburgh Compound B and Florbetapir: Comparing Radiotracers and Quantification Methods. *Journal of nuclear medicine : official publication, Society of Nuclear Medicine*. 2013;54(1):70-77.
20. Shoghi-Jadid K, Small GW, Agdeppa ED, Kepe V, Ercoli LM, Siddarth P, Read S, Satyamurthy N, Petric A, Huang SC, Barrio JR. Am J Geriatr Psychiatry. Localization of neurofibrillary tangles and beta-amyloid plaques in the brains of living patients with Alzheimer disease.2002 Jan-Feb;10(1):24-35.
21. Rupprecht R, Papadopoulos V, Rammes G, Baghai TC, Fan J, Akula N, Groyer G, Adams D, Schumacher M. Translocator protein (18 kDa) (TSPO) as a therapeutic target for neurological and psychiatric disorders. Nat Rev Drug Discov. 2010;9:971–988
22. Venneti S, Lopresti BJ, Wiley CA. Molecular imaging of microglia/macrophages in the brain. *Glia*. 2013;61(1):10-23. doi:10.1002/glia.22357.
23. Thiel A, Heiss WD. Imaging of microglia activation in stroke. Stroke. 2011 Feb;42(2):507-12.
24. Chauveau F, Boutin H, Van Camp N, Dolle F, Tavitian B. Nuclear imaging of neuroinflammation: a comprehensive review of [11C]PK11195 challengers. Eur J Nucl Med Mol Imaging. 2008;35:2304–2319.
25. Jalbert JJ, Daiello LA, Lapane KL. Dementia of the Alzheimer type. Epidemiol Rev. 2008;30:15-34. doi: 10.1093/epirev/mxn008. Epub 2008 Jul 16.
26. Sabuncu MR, Desikan RS, Sepulcre J, et al. The Dynamics of Cortical and Hippocampal Atrophy in Alzheimer Disease. Archives of neurology. 2011;68(8):1040-1048. doi:10.1001/archneurol.2011.167.
27. Mascalchi M, Lolli F, Della Nave R, Tessa C, Petralli R, Gavazzi C, Politi LS, Macucci M, Filippi M, Piacentini S. Huntington disease: volumetric, diffusion-weighted, and magnetization transfer MR imaging of brain. Radiology. 2004 Sep;232(3):867-73. Epub 2004 Jun 23.
28. Filippi M, Rocca MA. MR imaging of multiple sclerosis. Radiology. 2011 Jun;259(3):659-81. doi: 10.1148/radiol.11101362.
29. Ge Y. Multiple sclerosis: the role of MR imaging. AJNR Am J Neuroradiol. 2006 Jun-Jul;27(6):1165-76.
30. Tuite PJ, Mangia S, Michaeli S. Magnetic Resonance Imaging (MRI) in Parkinson's Disease. Journal of Alzheimer's disease & Parkinsonism. 2013;Suppl 1:001-. doi:10.4172/2161-0460.S1-001.

31. Schwarz ST, Afzal M, Morgan PS, Bajaj N, Gowland PA, Auer DP (2014) The 'Swallow Tail' Appearance of the Healthy Nigrosome – A New Accurate Test of Parkinson's Disease: A Case-Control and Retrospective Cross-Sectional MRI Study at 3T. PLoS ONE 9(4): e93814. doi:10.1371/journal.pone.0093814
32. Ransohoff RM, Kivisäkk P, Kidd G. Three or more routes for leukocyte migration into the central nervous system. Nat Rev Immunol. 2003 Jul;3(7):569-81.
33. Wilson EH, Weninger W, Hunter CA. Trafficking of immune cells in the central nervous system. J Clin Invest. 2010 May;120(5):1368-79. doi: 10.1172/JCI41911. Epub 2010 May 3.
34. Ceulemans A-G, Zgavc T, Kooijman R, Hachimi-Idrissi S, Sarre S, Michotte Y. The dual role of the neuroinflammatory response after ischemic stroke: modulatory effects of hypothermia. Journal of Neuroinflammation. 2010;7:74. doi:10.1186/1742-2094-7-74.
35. Ferretti MT, Merlini M, Späni C, Gericke C, Schweizer N, Enzmann G, Engelhardt B, Kulic L, Suter T, Nitsch RM. T-cell brain infiltration and immature antigen-presenting cells in transgenic models of Alzheimer's disease-like cerebral amyloidosis. Brain Behav Immun. 2016 Feb 9. pii: S0889-1591(16)30030-7.
36. Man S, Ubogu EE, Ransohoff RM. Inflammatory cell migration into the central nervous system: a few new twists on an old tale. Brain Pathol. 2007 Apr;17(2):243-50.
37. McAteer MA, Akhtar AM, von zur Muhlen C, Choudhury RP. An approach to molecular imaging of atherosclerosis, thrombosis, and vascular inflammation using microparticles of iron oxide. Atherosclerosis. 2010;209(1):18-27. doi:10.1016/j.atherosclerosis.2009.10.009.
38. Zimny A, Neska-Matuszewska M, Bladowska J, Sąsiadek MJ. Intracranial Lesions with Low Signal Intensity on T2-weighted MR Images – Review of Pathologies. Polish Journal of Radiology. 2015;80:40-50. doi:10.12659/PJR.892146.
39. Pagoto A, Stefania R, Garello F, Arena F, Digilio G, Aime S, Terreno E. Paramagnetic Phospholipid-Based Micelles Targeting VCAM-1 Receptors for MRI Visualization of Inflammation. Bioconjug Chem. 2016 Aug 17;27(8):1921-30.
40. Anelli, P. L., Lattuada, L., Lorusso, V., Schneider, M., Tournier, H., and Uggeri, F. Mixed micelles containing lipophilic gadolinium complexes as MRA contrast agents. *MAGMA.* 2001 12, 114– 20.
41. Vaccaro, M., Mangiapia, G., Paduano, L., Gianolio, E., Accardo, A., Tesauro, D., and Morelli, G. Structural and relaxometric characterization of peptide aggregates containing gadolinium complexes as potential selective contrast agents in MRI. *ChemPhysChem* 8, 2526– 38, DOI: 10.1002/cphc.200700505
42. Körbelin J, Dogbevia G, Michelfelder S, Ridder DA, Hunger A, Wenzel J, Seismann H, Lampe M, Bannach J, Pasparakis M, Kleinschmidt JA, Schwaninger M, Trepel M. A brain microvasculature endothelial cell-specific viral vector with the potential to treat neurovascular and neurological diseases. EMBO Mol Med. 2016 Jun 1;8(6):609-25. doi: 10.15252/emmm.201506078.
43. Hohlfeld R, Kerschensteiner M, Meinl E. Dual role of inflammation in CNS disease. Neurology. 2007;68:S58–63.
44. Pulli B, Chen JW. Imaging Neuroinflammation – from Bench to Bedside. Journal of clinical & cellular immunology. 2014;5:226. doi:10.4172/2155-9899.1000226.
45. McAteer MA, Sibson NR, von Zur Muhlen C, Schneider JE, Lowe AS, et al. In vivo magnetic resonance imaging of acute brain inflammation using microparticles of iron oxide. Nat Med. 2007;13:1253–1258.

46. Hoyte LC, Brooks KJ, Nagel S, Akhtar A, Chen R, et al. Molecular magnetic resonance imaging of acute vascular cell adhesion molecule-1 expression in a mouse model of cerebral ischemia. J Cereb Blood Flow Metab. 2010;30:1178–1187.
47. Serres S, Soto MS, Hamilton A, McAteer MA, Carbonell WS, et al. Molecular MRI enables early and sensitive detection of brain metastases. Proc Natl Acad Sci U S A. 2012;109:6674–6679.
48. Zimny A, Neska-Matuszewska M, Bladowska J, Sąsiadek MJ. Intracranial Lesions with Low Signal Intensity on T2-weighted MR Images – Review of Pathologies. Polish Journal of Radiology. 2015;80:40-50. doi:10.12659/PJR.892146.
49. Chen JW, Breckwoldt MO, Aikawa E, Chiang G, Weissleder R. Myeloperoxidase-targeted imaging of active inflammatory lesions in murine experimental autoimmune encephalomyelitis. Brain. 2008 Apr;131(Pt 4):1123-33.
50. Jesse V Jokerst, Tatsiana Lobovkina, Richard N Zare, Sanjiv S Gambhir. Nanoparticle PEGylation for imaging and therapy. Nanomedicine (Lond). 2011 Jun; 6(4): 715–728.
51. REF NANOMEDICINA TARGET (ENZO)
52. Kedar U, Phutane P, Shidhaye S, Kadam V. Advances in polymeric micelles for drug delivery and tumor targeting. Nanomedicine. 2010 Dec;6(6):714-29.
53. Al-Achi A, Jonathan Lawrence BS (2013) Micelles: Chemotherapeutic Drug Delivery. Clin Pharmacol Biopharm 2:e114.
54. Gaucher G, Satturwar P, Jones MC, Furtos A, Leroux JC.Eur J Pharm Biopharm. Polymeric micelles for oral drug delivery. 2010 Oct;76(2):147-58.

Electronic Supplementary Information

MRI visualization of neuroinflammation using VCAM-1 targeted paramagnetic micelles

Garello Francesca, [1] Pagoto Amerigo, Arena Francesca, Buffo Annalisa,[2,3] Alberti Diego, and Terreno Enzo[1]

[1] Molecular & Preclinical Imaging Centers,
Department of Molecular Biotechnology and Health Sciences,
University of Torino, Via Nizza 52,
10126 Torino, Italy

[2] Department of Neuroscience Rita Levi-Montalcini,
University of Turin,
10126 Turin, Italy

[3] Neuroscience Institute Cavalieri Ottolenghi,
Regione Gonzole 10,
10043 Orbassano, Turin, Italy

Table of Contents

Ex-vivo investigation of inflammatory hallmarks

The model of neuroinflammation obtained after the intra-striatal injection of LPS was characterized *ex-vivo*. More in details (n=1) animal was sacrificed 24 hours post injection, the brain excised and frozen at -80°C. Slices (20 µm thickness) were cut using a Leica CM 1950 cryostat and fixed in absolute ethanol for 5 min. Then some slices underwent hematoxylin and eosin (H&E) staining to evaluate the presence and entity of inflammation. As displayed in Figure S1a, the inflammatory process is quite extended in the striatum but limited to the operated hemisphere. The remaining slices underwent staining with rat anti mouse VCAM-1 antibody to evaluate the expression of the adhesion molecule in the striatum. More in details, following fixation in ethanol, slices were washed in PBS and then blocking with 10% goat serum was performed for 1h at room temperature. Subsequently the primary antibody was added to the slices in 10% goat serum and left overnight at 4°C (1:100 dilution). The day after the slices were rinsed in PBS and staining with the secondary antibody (1:500) Alexa Fluor 488 goat anti rat was carried out for 1 hour at room temperature. Three washings were performed to remove unbound material, and then nuclei were stained with Hoechst ($8x10^{-5}$ mg/mL, 10 min incubation). After a fast washing in bidistilled water, slices were mounted using ProLong® and imaged by confocal microscopy, magnification 40x, laser excitation 405 and 488 detect Hoechst and Alexa Fluor 488, respectively. Confocal microscopy images showed a remarkably higher expression of VCAM-1 in the inflamed striatum (Figure S1b), although a restricted signal could be detected also in some vessels in the contralateral one. As the inflammatory process was already in progress 24 hours post surgery (in literature it is reported to start from 16 hours post LPS administration) the animals were immediately recruited to maximize VCAM-1 detection at the onset of the inflammatory processes.

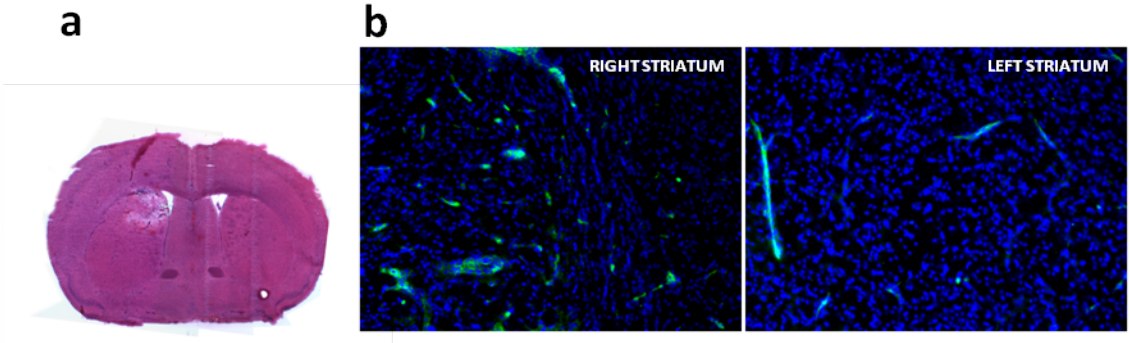

Figure S9. a) Hematoxylin and Eosin staining of C57BL/6J mouse brain 24 hours after the administration of 5 µg of LPS in the right striatum. A massive recruitment of immune system cells as well as diffuse edema are detectable in the operated striatum. b) Confocal microscopy images of brain slices of C57BL/6J mouse brain 24 hours after the administration of 5 µg of LPS in the right striatum. Nuclei are stained with Hoechst (Blue), VCAM-1 is displayed in green. A widespread expression of the cell adhesion molecule was detectable in the right striatum whereas a limited VCAM-1 staining is present in the contra-lateral one.

Biodistribution of VCAM-1 targeted micelles

The biodistribution of the system was investigated in the main excretory organs, both *in vivo*, by MRI at 20 min, 4h and 24 hours post injection, and *ex-vivo* by ICP-MS, through quantification of Gd(III) at 24 hours post micelle injection. As expected MRI data displayed a big accumulation of the particles in spleen and liver in the first hours post administration, as typically reported for nanosized objects.

At 24 hours post injection, instead, a steep decrease in liver and spleen was detectable in favor of accumulation in the site of inflammation (Figure S2).

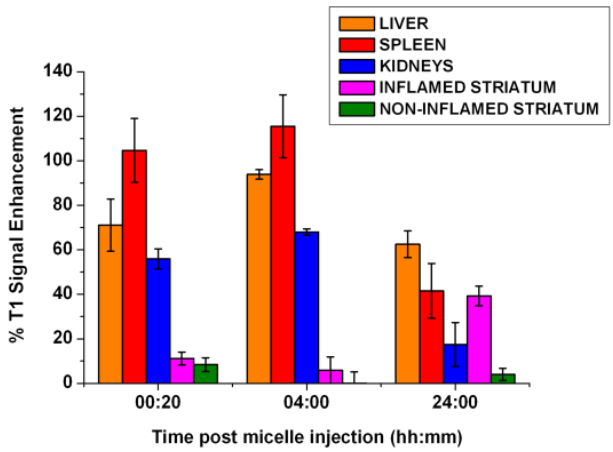

Figure S2. MRI contrast measured in different organs at various time points after the injection of paramagnetic micelles targeting VCAM-1 receptors. Blue bars refer to kidneys, red bars to spleen, orange bars to liver, purple bars to the inflamed striatum, green bars to the non-inflamed striatum. Error bars represent SE of the mean.

To confirm data obtained by MRI, soon after the end of the acquisition performed 24 hours post micelle injection, the animals were sacrificed and the organs excised, weighted and digested in concentrated nitric acid. After mineralization in microwave oven the samples were recollected in ultrapure water and analyzed by ICP-MS. Results obtained nicely agree with imaging data (Fig. S3). It should be mentioned that in the estimation of the Gd(III) content in the brain the quantification was carried out in the whole hemisphere instead of considering striatum only.

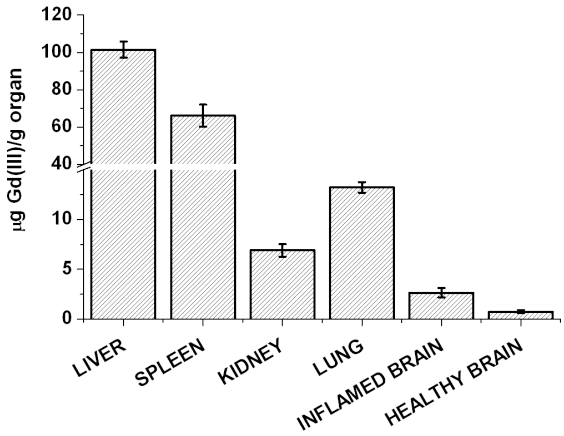

Figure S3. ICP-MS quantification of Gd(III) content in main excretory and target organs measured 24 hours post administration of VCAM-1 targeting micelles (n=7). Error bars represent SE of the mean.

Confocal microscopy images of VCAM-1 targeted micelles in the brain

Confocal microscopy images of left and right striatum were acquired 24 hours post injection of the targeted nanosystem. As displayed by MRI, a big accumulation of fluorescent micelles is detectable in the inflamed striatum, while only a few and sprinkled micelles are detectable in the contralateral, healthy, one (Figure S4).

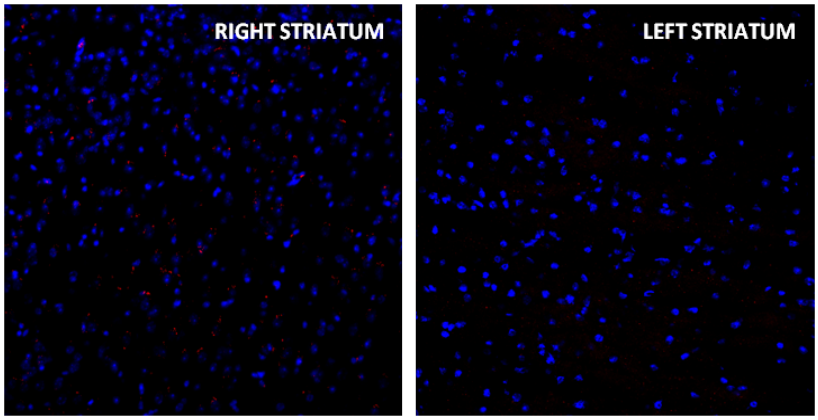

Figure S4. Confocal microscopy images of brain slices of C57BL/6J mouse brain 24 hours after the administration of micelles targeting VCAM-1. Nuclei are stained in blue, micelles are visible in red. While in the right striatum a high amount of the nanosystem is detectable, in the left striatum red spots are seldom.